Heliyon 10 (2024) e35004

Contents lists available at ScienceDirect

Heliyon

journal homepage: www.cell.com/heliyon

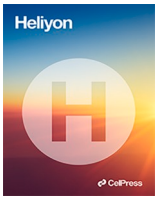

Research article

Construction of a prognostic model for ovarian cancer based on a comprehensive bioinformatics analysis of cuproptosis-associated long non-coding RNA signatures

Rujun Chen [a,1], Yating Huang [a,1], Ke Sun [a], Fuyun Dong [a], Xiaoqin Wang [a], Junhua Guan [a], Lina Yang [a,b,**], He Fei [a,*]

[a] Department of Gynecology and Obstetrics, Shanghai Fifth People's Hospital, Fudan University, Shanghai, 200240, PR China
[b] Central Laboratory, Shanghai Fifth People's Hospital, Fudan University, Shanghai, 200240, PR China

ARTICLE INFO

Keywords:
Cuproptosis
Prognostic model
Long non-coding RNAs signature
Patient survival
Immune infiltration

ABSTRACT

Ovarian cancer (OCa) is a common malignancy in women, and the role of cuproptosis and its related genes in OCa is unclear. Using the GSE14407 dataset, we analyzed the expression and correlation of cuproptosis-related genes (CRGs) between tumor and normal groups. From the TCGA-OV dataset, we identified 20 cuproptosis-related long non-coding RNAs (CuLncs) associated with patient survival through univariate Cox analysis. OCa patients were divided into early-stage and late-stage groups to analyze CuLncs expression. Cluster analysis classified patients into two clusters, with Cluster1 having a poorer prognosis. Significant differences in "Lymphatic Invasion" and "Cancer status" were observed between clusters. Seven CRGs showed significant expression differences, validated using the human protein atlas (HPA) databases. Immune analysis revealed a higher ImmuneScore in Cluster1. GSEA identified associated signaling pathways. LASSO regression included 11 CuLncs to construct and validate a survival prediction model, classifying patients into high-risk and low-risk groups. Correlations between riskScore, Cluster phenotype, ImmuneScore, and immune cell infiltration were explored. Cell experiments showed that knocking down AC023644.1 decreases OCa cell viability. In conclusion, we constructed an accurate prognostic model for OCa based on 11 CuLncs, providing a basis for prognosis assessment and potential immunotherapy targets.

Abbreviations: OCa, Ovarian cancer; CRGs, Cuproptosis-related genes; CuLncs, Cuproptosis-related lncRNAs; TCGA, The Cancer Genome Atlas; HPA, human protein atlas; KEGG, Kyoto Encyclopedia of Genes and Genomes.

* Corresponding author. Department of Gynecology and Obstetrics, Shanghai Fifth People's Hospital, Fudan University, No.801 Heqing Road, Minhang District, Shanghai, 200240, PR China.

** Corresponding author. Department of Obstetrics and Gynecology & Central laboratory, Shanghai Fifth People's Hospital, Fudan University, No.801 Heqing Road, Minhang District, Shanghai, 200240, PR China.

E-mail addresses: chenrujun@fudan.edu.cn (R. Chen), 13162269121@163.com (Y. Huang), sunke1123@163.com (K. Sun), 254970372@qq.com (F. Dong), 15000918619@163.com (X. Wang), 18918168587@163.com (J. Guan), linayang12@fudan.edu.cn (L. Yang), sunshinefh809@163.com (H. Fei).

[1] Contributed equally.

https://doi.org/10.1016/j.heliyon.2024.e35004
Received 7 March 2024; Received in revised form 19 July 2024; Accepted 22 July 2024
Available online 23 July 2024

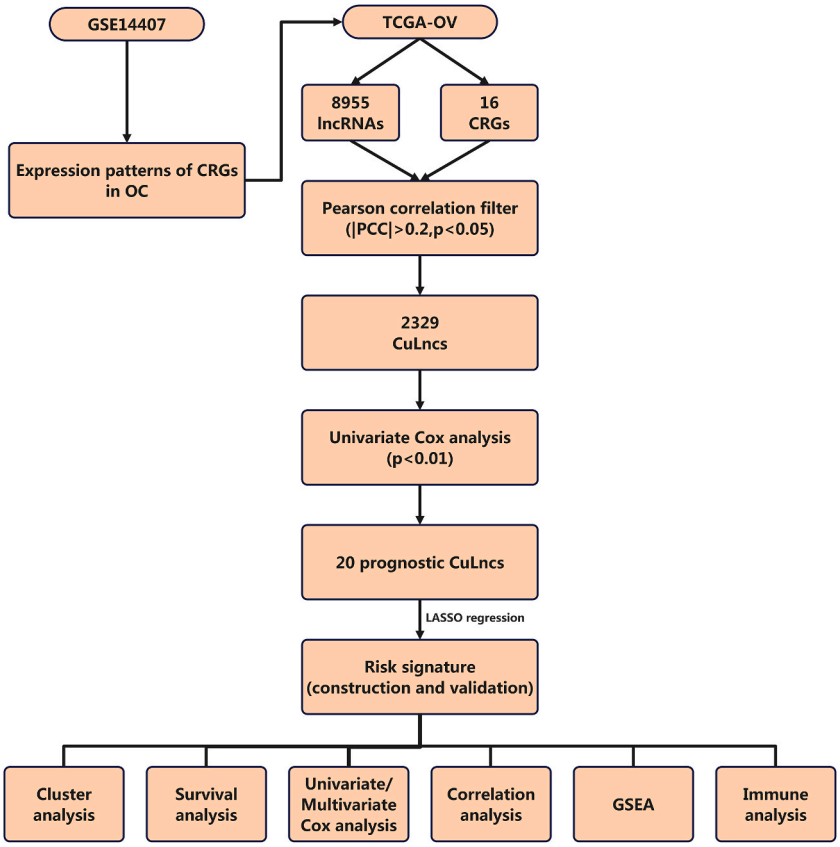

Fig. 1. Flowchart of the study.

1. Introduction

In the female reproductive system, ovarian cancer (OCa) is one of the most common malignant tumors [1]. Cuproptosis, a form of regulated cell death associated with copper metabolism, has recently gained attention as a critical mechanism implicated in various pathological conditions, including cancer [2]. Long non-coding RNAs (lncRNAs), a class of non-coding RNA molecules, have emerged as important regulators of gene expression and cellular processes [3]. Increasing evidence suggests a significant interplay between cuproptosis and lncRNAs, with profound implications in the development and progression of multiple cancers [4–7].

In the context of OCa, both cuproptosis and lncRNAs have been shown to play critical roles in tumor development, progression, and treatment response [2,8,9]. Dysregulation of cuproptosis has been observed in OCa cells, with abnormal copper metabolism contributing to increased cell survival and chemoresistance [10,11]. Several lncRNAs have been identified as key regulators of cuproptotic cell death, affecting the expression of copper-related genes and modulating the sensitivity of OCa to cuproptosis-inducing agents [6,12].

The purpose of this study is to construct a comprehensive bioinformatics-based model that integrates the signature of cuproptosis-related lncRNAs, immune infiltration profiles, and survival prognostic factors for OCa. By utilizing various bioinformatics approaches, we aim to identify a specific set of cuproptosis-related lncRNAs that are associated with the pathogenesis and progression of OCa. Additionally, we will assess the immune infiltration patterns in OCa and investigate their correlation with the expression of cuproptosis-related lncRNAs. Ultimately, our goal is to establish a robust prognostic model that can predict the survival outcomes of OCa patients, providing valuable insights for personalized therapeutic strategies and improving patient management. As shown in Fig. 1, an overview of the research design is provided.

2. Materials and methods

2.1. Data acquisition

The dataset, with the accession number GSE14407, was obtained from the GEO database (https://www.ncbi.nlm.nih.gov/geo). It includes gene expression microarray data for 12 cases of OCa and 12 cases of normal ovarian epithelium. The gene expression RNAseq (HTSeq-FPKM), clinicopathological data, survival data, and mutation data for OCa were downloaded from The Cancer Genome Atlas

(TCGA) online database (https://cancergenome.nih.gov). To ensure fairness in the analysis, the data of 429 cases from TCGA-OV patients were randomly divided into a training set and an internal verification set, maintaining a 1:1 ratio between the two sets. The appropriateness of the grouping was validated using a Chi-square test.

2.2. Identification of the cuproptosis-related lncRNAs (CuLncs)

We obtained 16 cuproptosis-related genes (CRGs) from previous articles [13,14](Table S1). The TCGA-OV transcriptome data was filtered and processed using the R software. We extracted transcriptome data from 429 tumor samples, filtering out genes that showed no expression in less than half of the samples. From this data, we extracted the expression information for CRGs as well as the expression information for all lncRNAs. By performing a Spearman's correlation analysis on the expression profiles of CRGs and lncRNAs, we obtained an expression matrix specifically for cuproptosis-related lncRNAs, referred to as CuLncs. The statistical significance level was set at FDR-adjusted $P < 0.05$ in order to determine the significance of the correlations.

2.3. Cluster analysis of the cuproptosis-related lncRNAs

Univariate Cox analysis was performed using the 'survival' package [15] in R software to identify CuLncs significantly associated with the survival of OCa patients. A significance level of $P < 0.01$ was used to determine the statistical significance. Furthermore, cluster analysis was conducted using the 'ConsensusClusterPlus' package [16] in R. The analysis was set with $k = 2$, and based on the expression levels of CuLncs associated with survival, TCGA-OV patients were classified into two categories, namely cluster 1 and cluster 2.

2.4. Construction and validation of the cuproptosis-related lncRNAs prognostic signature

To construct a more refined prognostic model for OCa survival prediction, LASSO Cox regression analysis was performed using these CuLncs significantly associated with survival in the training set. The risk score of each OCa patient was calculated as follows: Risk score $= \sum$ (coefficients $\times$ gene expression). Subsequently, all OCa cases were divided into low-risk or high-risk groups according to the values below or above the median risk score, and the survival curves of the two groups were plotted by the Kaplan-Meier method [17]. In addition, a time-dependent receiver operating characteristic (ROC) curve was generated using the "timeROC" package [18] to assess the prognostic signature's effectiveness in predicting 1-year, 3-year, and 5-year survival. A heatmap for both high-risk and low-risk groups was generated using the "pheatmap" package [19]. Furthermore, clinical parameters including Age, Stage, Grade, and the risk score were incorporated, and both univariate and multivariate Cox analyses were conducted. Forest plots were then constructed to visualize the results. Finally, the survival model was validated using the validation cohort.

2.5. Identification of relevant signaling pathways of cuproptosis-related genes by GSEA

Functional enrichment analysis of the Kyoto Encyclopedia of Genes and Genomes (KEGG) was performed using the GSEA tool [20] (version 4.3.2) with data obtained from the TCGA database. The gene set parameters and enrichment test settings were configured as follows. The expression dataset was named after each gene, and the gene sets database chosen was "c2.cp.kegg.v2022.1.Hs.symbols.gmt". A default value of 1000 permutations was employed to compute the Normalized Enrichment Score (NES). Additionally, a maximum size threshold of 500 and a minimum size threshold of 15 were applied to exclude larger and smaller gene sets, respectively. Significant enrichment was determined by a false discovery rate (FDR) q-value <0.05. When the q-value exceeded 0.05, signaling pathways with a P-value <0.05 were selected for enriched analysis. In cases where no signaling pathway had a P-value <0.05, the maximum size threshold for excluding larger sets was adjusted to 600 or 700.

2.6. Screening of cuproptosis-related genes and validation in human protein atlas (HPA) databases

To investigate the differentially expressed mRNA in CRGs, the 'limma' package [21] in the R software was utilized. A threshold of adjusted $P < 0.05$ was established to identify mRNAs exhibiting significant differential expression between two clusters. The protein expression of cuproptosis-related genes, which were identified through the screening process, was assessed in both OCa tissues and normal ovarian tissues using the HPA portal (https://www.proteinatlas.org/).

2.7. Tumor microenvironment analysis

The abundance of immune infiltrates was estimated using the "CIBERSORT" [22] and "estimate" packages in R. To further analyze the differences between Cluster 1 and Cluster 2, the ESTIMATEScore, ImmuneScore, and StromalScore were separately calculated. The analysis of differential expression between the two clusters was conducted using the limma package, with a significance threshold set at $P < 0.05$. Additionally, violin plots depicting the infiltration of 22 immune cell types, including B cells, Plasma cells, T cells, NK cells, Monocytes, among others, between Cluster 1 and Cluster 2, were generated using the "limma" and "vioplot" [23] packages.

Table 1
Primers used in this study.

Primer name	Sequence (5′-3′)
GAPDH-hF	TGACAACTTTGGTATCGTGGAAGG
GAPDH-hR	AGGCAGGGATGATGTTCTGGAGAG
AC023644.1-hF	GTGGTAGTCAGGCAATGATTACAG
AC023644.1-hR	CTTGTACTCCGTCAGCGTGA

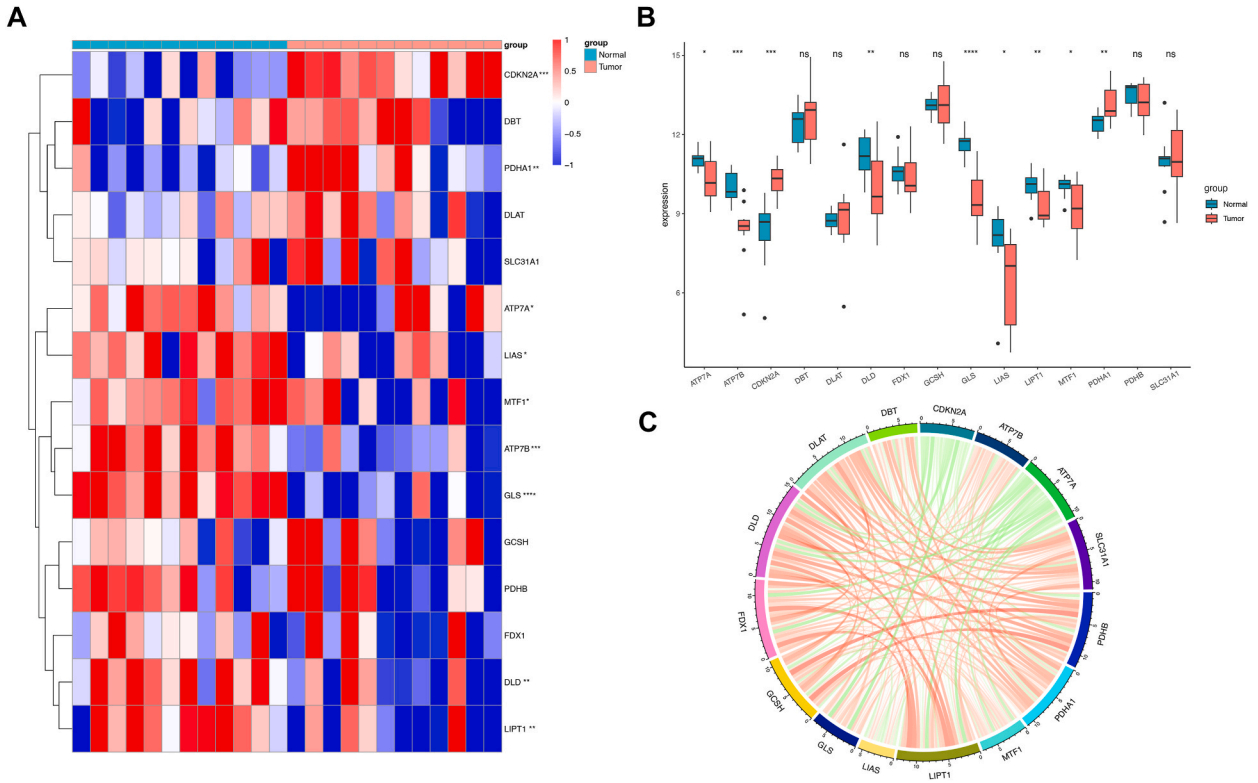

Fig. 2. Expression and correlation of cuproptosis-related genes in OV and normal group. Heatmap (A) and boxplot (B) of the expression profiles of cuproptosis-related genes in the tumor group and normal group. The transfection efficiency was confirmed by Western blot analysis. (C) Correlation analysis of gene expression levels of cuproptosis-related genes in OV. Red represents positive correlation, while green represents negative correlation. ns: non-significant; *P < 0.05, **P < 0.01, ***P < 0.001, ****P < 0.0001.

2.8. Correlation analysis

Correlation analysis was performed between riskScore and 22 immune cell types, based on Spearman's correlation method. A significance level of FDR-adjusted $P < 0.05$ was considered statistically significant. The "ggplot2" package [24] was utilized to generate scatter plots visualizing the correlation.

2.9. Cell cultivation and reagents

The human ovarian cancer epithelial cell lines (A2780 and SKOV3) were obtained from the American Type Culture Collection. The human normal ovarian epithelial cells (T29) have been described previously [25]. These cells were systematically nurtured in RPMI 1640 + 2 mM Glutamine +10 % fetal bovine serum (FBS), maintaining a controlled environment at 37 °C with a 5 % concentration of carbon dioxide (CO^2). Elesclomol (S80741) were purchased from Shanghai yuanye Bio-Technology Co., Ltd. Cupric chloride (C106775-1g) was purchased from Aladdin.

2.10. Cell transfection procedures

Three small interference RNAs (siRNAs) was designed and synthesized in Jiangsu Genecefe Biotechnology Co., Ltd. The siRNA sequences were as follows: siRNA-1 (5′-GACACUUUCUACAUCUUGATT-3′), siRNA-2 (5′-GGCACUGAAGGCACUACAATT-3′), and

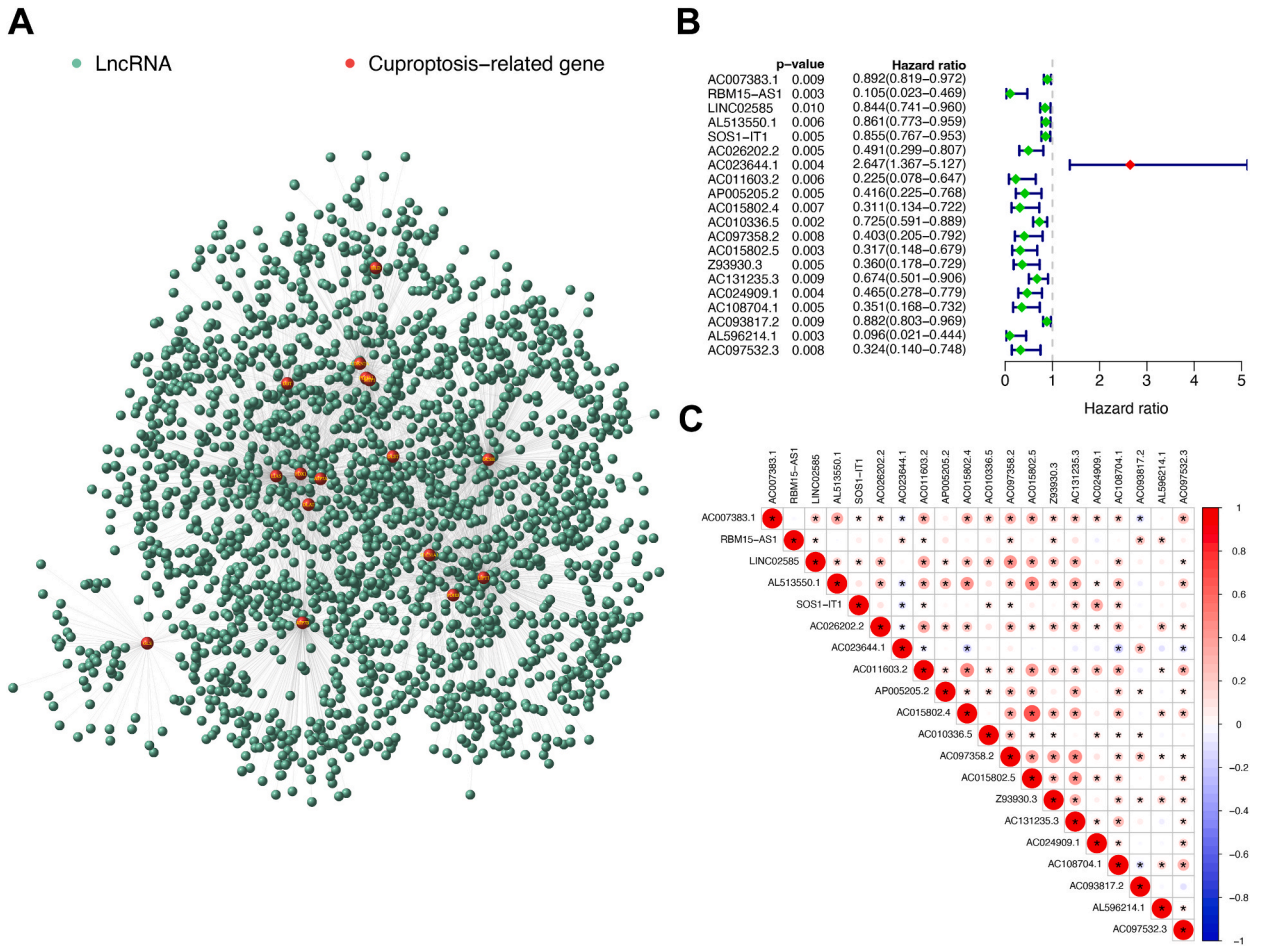

Fig. 3. Screening of survival-related cuproptosis-associated lncRNAs and analysis of their expression correlation. (A) Network diagram of the correlation between cuproptosis-related genes and lncRNAs. Red represents cuproptosis-related genes, while green represents lncRNAs. (B) Identification of survival-related cuproptosis-associated lncRNAs using univariate Cox analysis. (C) Analysis of expression correlation among survival-related cuproptosis-associated lncRNAs. Red represents cuproptosis-related genes, while blue represents lncRNAs. *$P < 0.05$.

siRNA-3 (5′-CCCUGUUGCUGACAGGUUATT-3′). A non-targeting siRNA was employed as the negative control. Transfections were carried out using Lipofectamine® 2000 Transfection Reagent (Thermo) in accordance with the manufacturer's instructions. Cellular specimens were collected for subsequent experiments 48 h post-transfection.

2.11. Reverse transcription-quantitative PCR (RT-qPCR) assay

Total RNA extraction employed RNAiso Plus (Takara Bio, Inc.). PrimeScript™ RT Master Mix (Takara Bio, Inc.) was used for reverse transcription, and SYBR Premix Ex Taq (Takara Bio, Inc.) facilitated RT-qPCR. A LongGene® Real-Time PCR System Q2000B (LongGene) was used for qPCR, with GAPDH as a reference gene. Primer sequences are provided in Table 1.

2.12. Cell counting kit-8 (CCK-8) assay

Cells were seeded at a density of 1×10^4 per well in a 96-well plate, mixed thoroughly, and incubated overnight. The next day, transfection was performed. Six hours post-transfection, the medium was replaced with varying concentrations of Elesclomol-Cu (0 nM, 20 nM, 40 nM, 60 nM, 80 nM). After 24 h of drug treatment, 10 μl of CCK-8 solution was added to each well. The plates were then incubated in the incubator for 1–4 h, and the OD value was measured at 450 nm using a microplate reader (Molecular Devices, LLC).

2.13. Statistical analysis

The statistical analysis and data visualization were performed using R (version 4.1.2) (https://www.r-project.org/). Spearman's correlation method was used for correlation analysis. Comparison of parameters between two or more groups was conducted using the

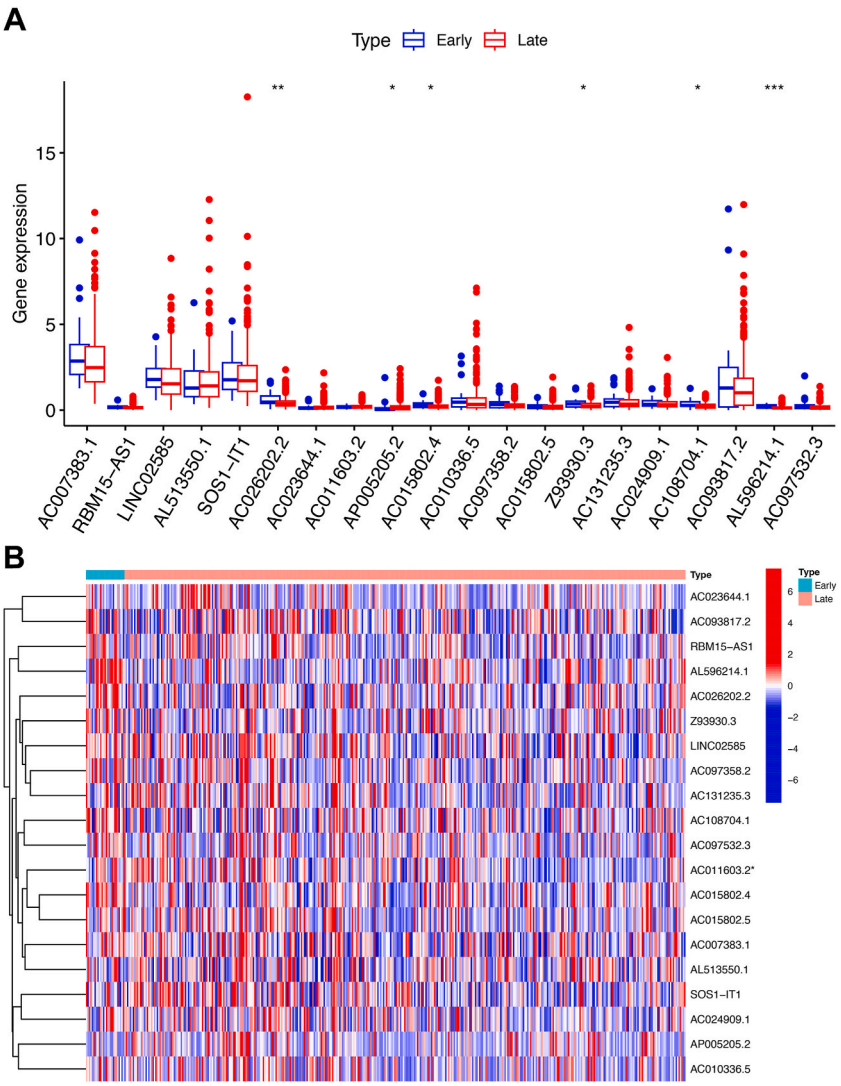

Fig. 4. Expression patterns of cuproptosis-associated lncRNAs in early and late-stage OCa. Boxplot (A) and heatmap (B) of cuproptosis-associated lncRNA expression levels were generated for the early-stage and late-stage OCa groups. *P < 0.05, **P < 0.01, ***P < 0.001.

Wilcoxon test. The FDR method was used to correct the *P*-value for the multiple tests. The *P*-values were calculated using a two-tailed test, and a significance threshold of $P < 0.05$ was considered statistically significant.

3. Results

3.1. Expression patterns of cuproptosis-related genes in OCa

Obtaining the GSE14407 data set, we found that 9 CRGs showed significant differences in the comparison between the OCa and the normal ovarian tissue through gene expression differential analysis (Fig. 2A and B). In addition, the results of co-expression analysis showed that the expression of most CRGs was positively correlated, while the expression of CDKN2A and ATP7A was negatively correlated (Fig. 2C).

3.2. Identification and screening of cuproptosis-related lncRNAs

First, we identified 2329 CuLncs significantly associated with the expression of 16 CRGs in TCGA-OV tumor samples (Fig. 3A). Next, we screened 20 CuLncs that were eligible and associated with survival using univariate Cox analysis. Among them, except for AC023644.1, which was an unfavorable factor for the survival of OCa patients, the other 19 CuLncs were all associated with good survival (Fig. 3B). Furthermore, the correlation analysis results showed that most of the expressions of the 20 CuLncs were positively

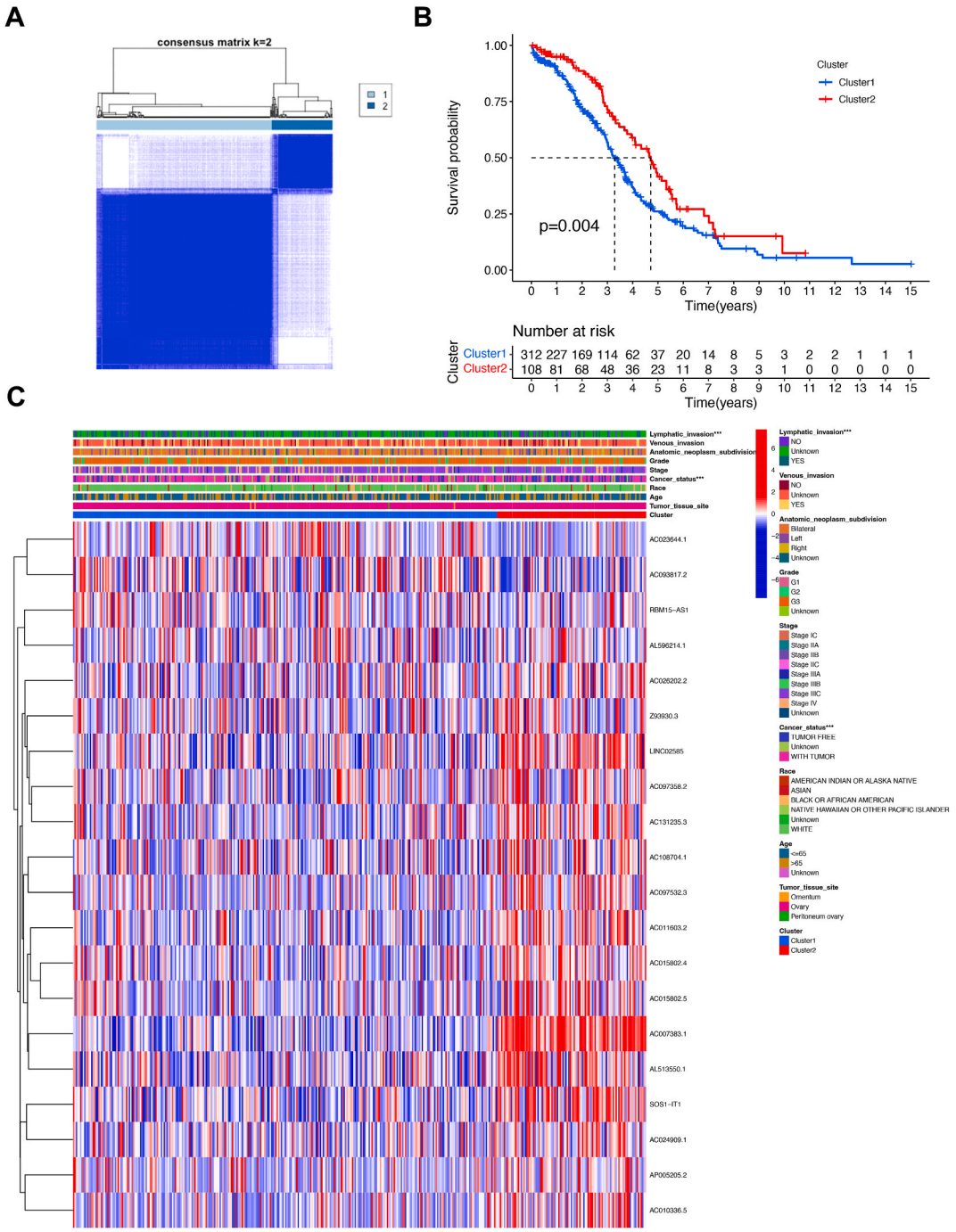

Fig. 5. Expression pattern, survival analysis, and correlation with clinical and pathological parameters of cuproptosis-associated lncRNAs in two OCa clusters. (A) Consensus clustering matrix for k = 2. (B) The Kaplan-Meier curves depict the survival rates of two clusters of OV patients. (C) The expression pattern of lncRNAs in two clusters is visualized through a heatmap, along with the correlation analysis between lncRNAs and various clinical pathological parameters. ***P < 0.001.

correlated with each other (Fig. 3C).

3.3. Differences in CuLncs expression in early and late stages of OCa

We divided OCa samples into early group (stage I, II) and late group (III, IV) according to clinical stage. In the comparison of expression between the two groups, there were significant differences in 6 CuLncs, including: AC026202.2, AP005205.2, AC015802.4,

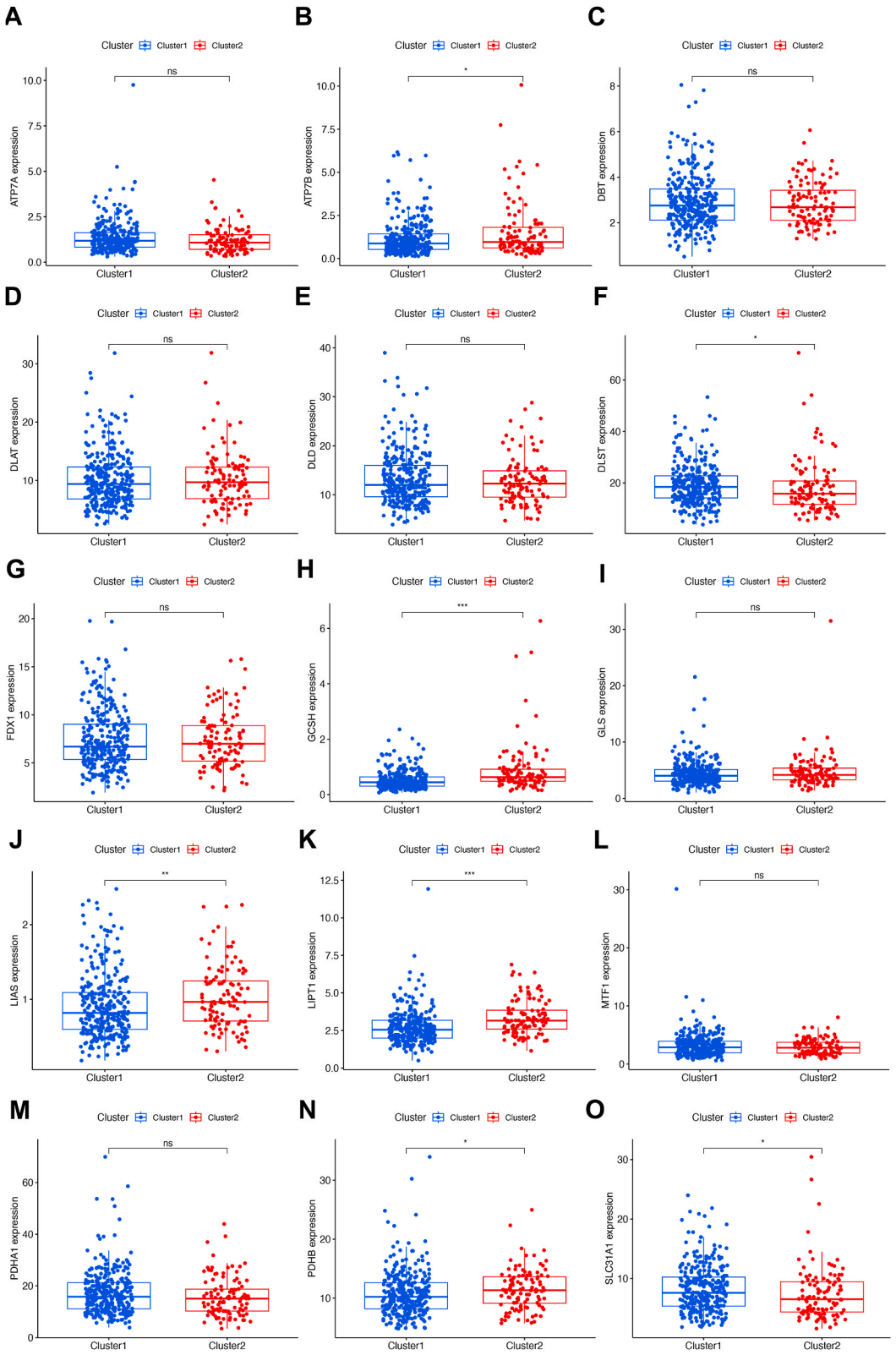

Fig. 6. Differential expression of cuproptosis-associated genes between the two clusters of OV patients. ns: non-significant; *P < 0.05, **P < 0.01, ***P < 0.001.

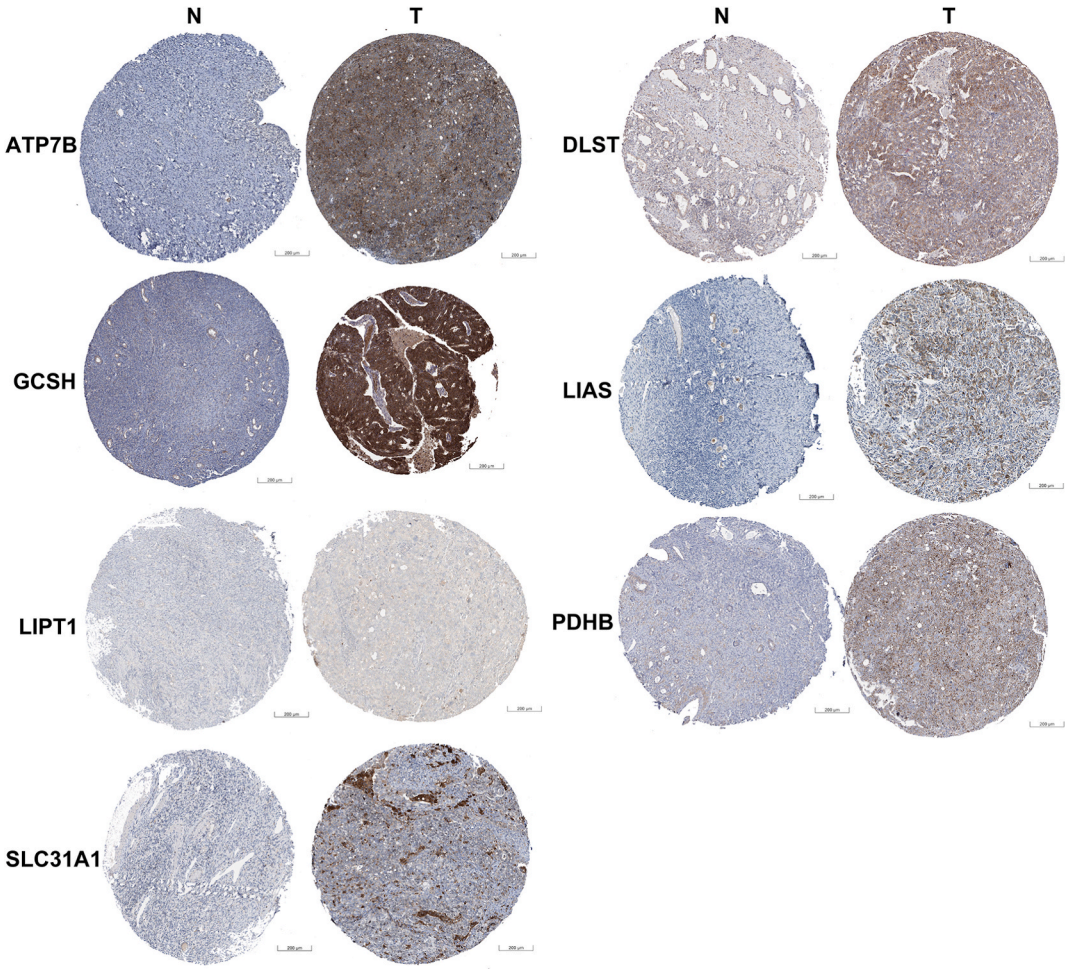

Fig. 7. Differential protein expression of cuproptosis-related genes in OV and normal ovarian tissues explored by immunohistochemical analysis.

Z93930.3, AC108704.1 and AL596214.1 (Fig. 4A). In Fig. 4B, the heatmap shows the different expression patterns of CuLncs between early and late groups.

Identification of cuproptosis subtypes in OCa and comparison of survival and clinicopathological parameters between the two subtypes.

Using the Consensus Cluster Plus package in R, we set k = 2, and finally divided the TCGA-OV samples into cluster 1 and cluster 2 based on the expression of 20 CuLncs (Fig. 5A). Moreover, survival analysis showed that the survival of OCa patients in cluster 1 was significantly worse than that in cluster 2 (Fig. 5B). Based on the cuproptosis subtypes, the clinicopathological parameters of OCa patients were analyzed, and the results showed that there were significant differences in 'Lymphatic invasion' and 'Cancer status' (Fig. 5C).

3.4. Differences in expression of CRGs in cuproptosis subtypes

In order to explore the expression of CRGs in the two cuproptosis subtypes, we performed differential analysis of CRGs expression. The results of gene expression differential analysis showed that there were significant differences in the expression of 7 CRGs in the two cuproptosis subtypes (Fig. 6A–O). It was found that the mRNA expression of DLST and SLC31A1 in Cluster 1 subtype was significantly higher than that in Cluster 2 subtype, while in Cluster 1 subtype, the mRNA expression level of ATP7B, GCSH, LIAS, LIPT1 and PDHB was significantly lower than that in Cluster 2 subtype. Moreover, it was shown in Fig. 7 that the protein levels of CRGs were different in the comparison between OCa group and normal ovarian tissue.

3.5. Analysis of the immune microenvironment based on cuproptosis subtypes

To investigate the immune microenvironment in two cuproptosis subtypes, we performed immune cell component analysis on the TCGA-OV dataset. Our results showed that there was no significant difference in the proportion of most immune cells in the immune

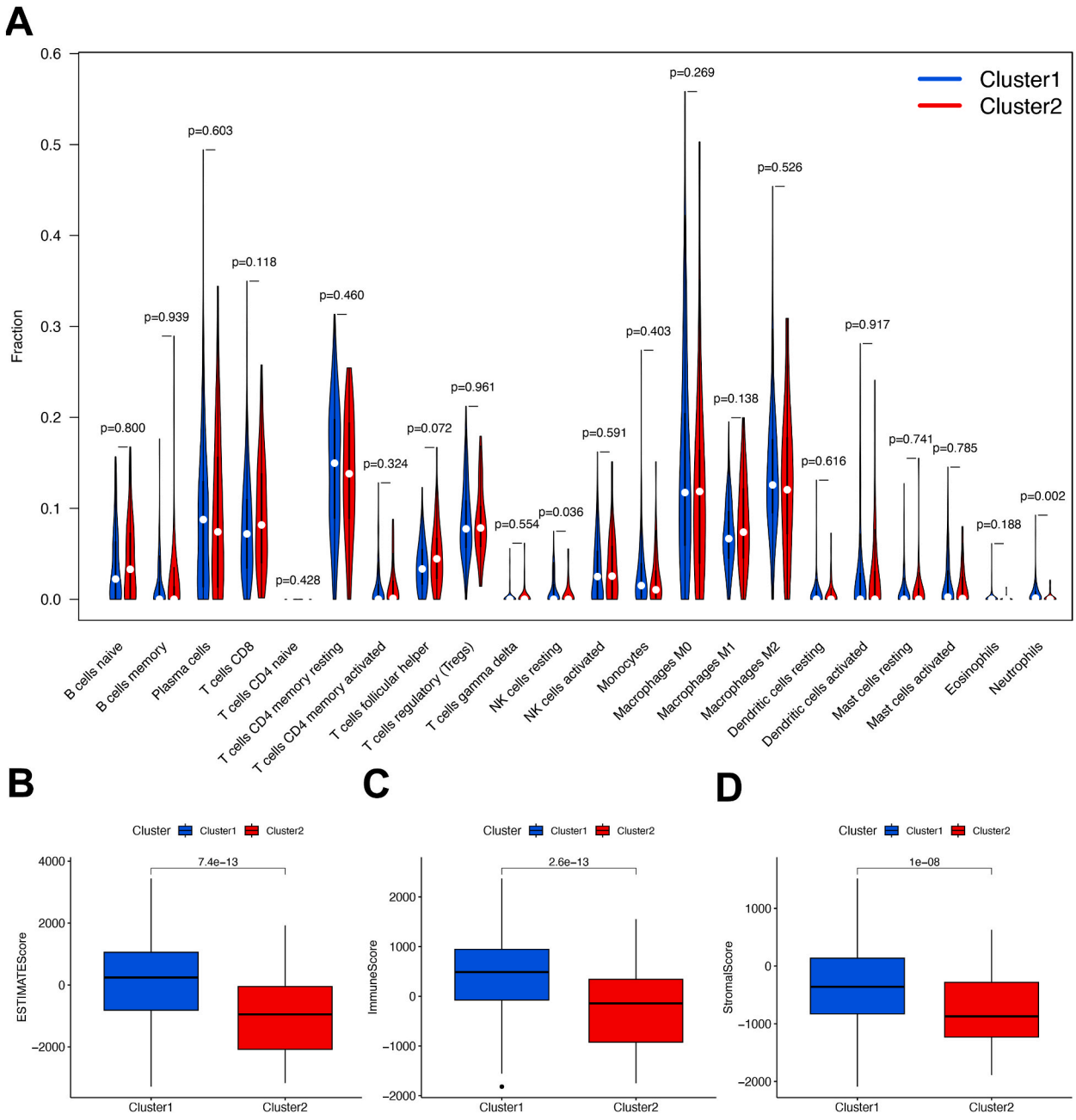

Fig. 8. Assessment of tumor immune microenvironment and evaluation of immune cell infiltration level between two clustering groups. (A) Infiltration status of 22 immune cells in the two clustering groups. (B) The ESTIMATEScore, ImmuneScore, and StromalScore show differences between the two clustering groups.

microenvironment of the two subtypes, except for NK cells resting and Neutrophils (Fig. 8A). However, the ESTIMATEScore, ImmuneScore, and StromalScore of Cluster 1 were significantly higher than those of Cluster 2 (Fig. 8B).

3.6. Biofunctional analysis based on cuproptosis subtypes

To further explore the enrichment of KEGG signaling pathways in the 2 cuproptosis subtypes, we performed GSEA. In Fig. 9A, there is a difference in gene expression pattern between Cluster 1 and Cluster 2. The enrichment analysis results showed that 146/175 gene sets were upregulated in phenotype Cluster 1 and 69 gene sets were significantly enriched at FDR <25 %. In addition, 29/175 gene sets were upregulated in phenotype Cluster 2 and 1 gene set was significant at FDR <25 %. The enrichment plots of the top 4 signaling

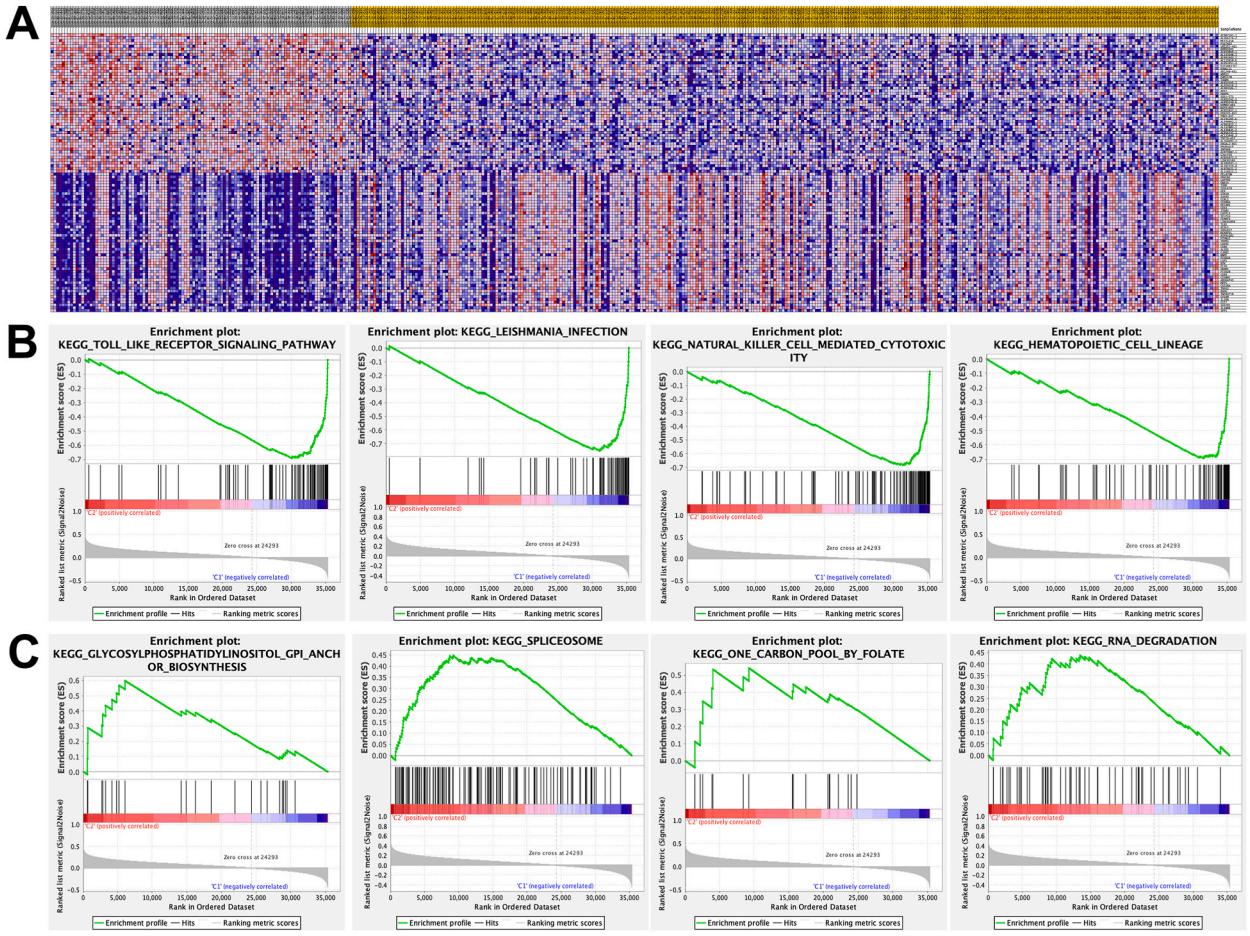

Fig. 9. Identification of relevant signaling pathways of cuproptosis-related genes by GSEA. (A) Heatmap of the top 50 features for each phenotype in two clusters. Top 4 KEGG pathways enrichment in Cluster1 (C) and Cluster2 (D) phenotype.

pathways in each subtype, including KEGG_NATURAL_KILLER_CELL_MEDIATED_CYTOTOXICITY, KEGG_SPLICEOSOME, KEGG_RNA_DEGRADATION, etc., were shown in Fig. 9B and C.

3.7. Construction and validation of the CuLncs prognostic signature

We developed a prognostic assessment model based on CuLncs. First, we randomly divided all patients into training group (n = 210) and validation group (n = 210) according to the ratio of 1:1. Then, LASSO analysis was used to select the optimal solution, and the remaining 11 CuLncs were screened, and the corresponding coefficients were calculated (Fig. 10A and B). Finally, the risk score calculation formula of the obtained cuproptosis-related prognostic model is as follows: Risk Score = RBM15-AS1 × −0.749717956 + AC026202.2 × −0.374835344 + AC023644.1 × 0.789732801 + AC011603.2 × −0.281841658 + AP005205.2 × −0.156860749 + AC010336.5 × −0.081330259 + AC015802.5 × −0.248389447 + AC024909.1 × −0.598428759 + AC108704.1 × −0.327142843 + AC093817.2 × −0.079123083 + AC097532.3 × −0.994617671. According to the risk score, patients were divided into high-risk group and low-risk group. In both training and validation groups, Kaplan-Meier curves showed that the survival of the high-risk group was worse than that of the low-risk group (Fig. 10C and D). It was shown in Fig. 10E, F that the prognostic model constructed by 11 CuLncs can accurately predict the survival of OCa patients at 1, 3, and 5 years, both in the training group and in the validation group. We found that the 11 CuLncs included in the prognostic model had significantly different expressions between the high-risk group and the low-risk group, that is, CuLncs except AC023644.1 showed low expression level in the high-risk group. This expression signature was consistent in the training set and in the validation set (Fig. 11A and B). As can be seen from the risk distribution plot, high-risk patients have shorter survival times in both the training and validation groups (Fig. 11C–F). The results of univariate and multivariate Cox regression analysis showed that both risk score and age were independent prognostic factors for patients with OCa (Fig. 11G–J).

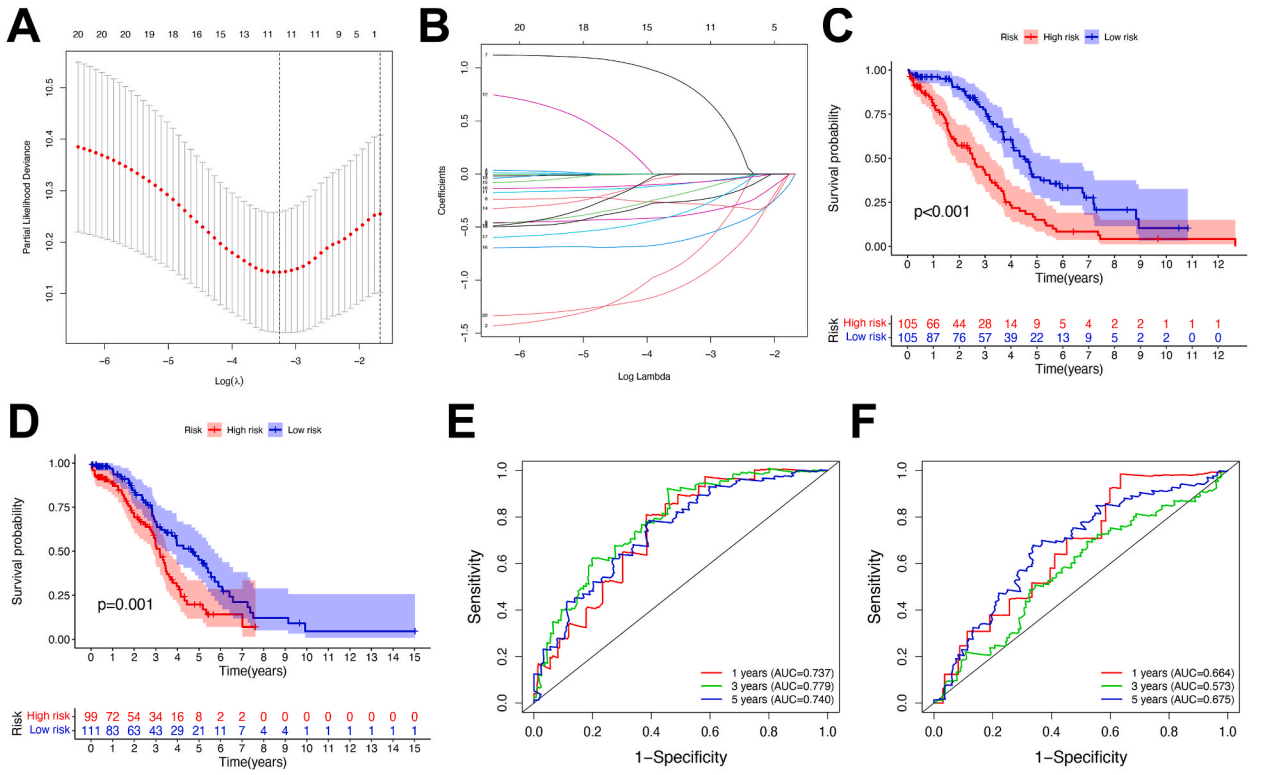

Fig. 10. Construction of an OCa survival prognostic model based on cuproptosis-related lncRNAs. (A, B) Using LASSO regression to converge the model, construct a streamlined OV survival prognosis model. Randomly divide the patients in the TCGA-OV cohort into training set (C) and validation set (D). Using the constructed survival prognosis prediction model, perform risk scoring for OV patients in both groups, distinguish high-risk and low-risk groups by the median value, and conduct survival analysis for each group. The ROC curve presents the AUC values for the 1-year, 3-year, and 5-year time points observed in both the training set (E) and validation set (F).

3.8. Clinicopathology analysis based on the risk model

We grouped OCa patients based on various clinicopathological parameters, and compared the risk values between the groups (Fig. 12A). We found that the risk value of Cluster1 was significantly higher than that of Cluster2 (Fig. 12B), the risk value of the high-ImmuneScore group was higher than that of the low-ImmuneScore group (Fig. 12C), and the risk value of the early group (stage I-II) is lower than the advanced group (stage III-IV) (Fig. 12D).

3.9. Differences in CRGs expression based on the risk model

We explored the expression of CRGs in the high-risk group and low-risk group, as shown in Fig. 13A–P. Among them, the expressions of GCSH, LIAS and LIPT1 were significantly different in the comparison between the two groups.

3.10. Immune infiltration based on the risk model

In order to further understand the relationship between immune cell infiltration and risk value in the tumor microenvironment, we conducted a correlation analysis, and the results showed that Macrophages M2 and Neutrophils were significantly positively correlated with riskScore (Fig. 14A and B), while Plasma cells and T cells follicular helper were significantly negatively correlated with riskScore (Fig. 14C and D).

Knocking down AC023644.1 inhibits the viability of OCa cells, but it is not sensitive to cuproptosis inducer.

Our findings indicate that AC023644.1 is a risk factor for poor prognosis in OCa patients. We hypothesize that AC023644.1 may play a role in inhibiting cuproptosis in OCa cells. To test this hypothesis, we first measured the expression levels of AC023644.1 in normal ovarian epithelial cells (T29) and ovarian cancer cells (A2780, HEYA8, SKOV3, OVCA433) using RT-qPCR. The results showed that, compared to T29 cells, the expression of AC023644.1 was significantly upregulated in A2780, HEYA8, and SKOV3 cells, while it was significantly downregulated in OVCA433 cells (Fig. 15A). Subsequently, we selected A2780 and SKOV3 cells, which showed notably higher AC023644.1 expression, for further studies. Next, we knocked down AC023644.1 in A2780 and SKOV3 cells using small interfering RNA (siRNA) (Fig. 15B). Finally, we constructed a cuproptosis gradient model in ovarian cancer cells using elesclomol, a

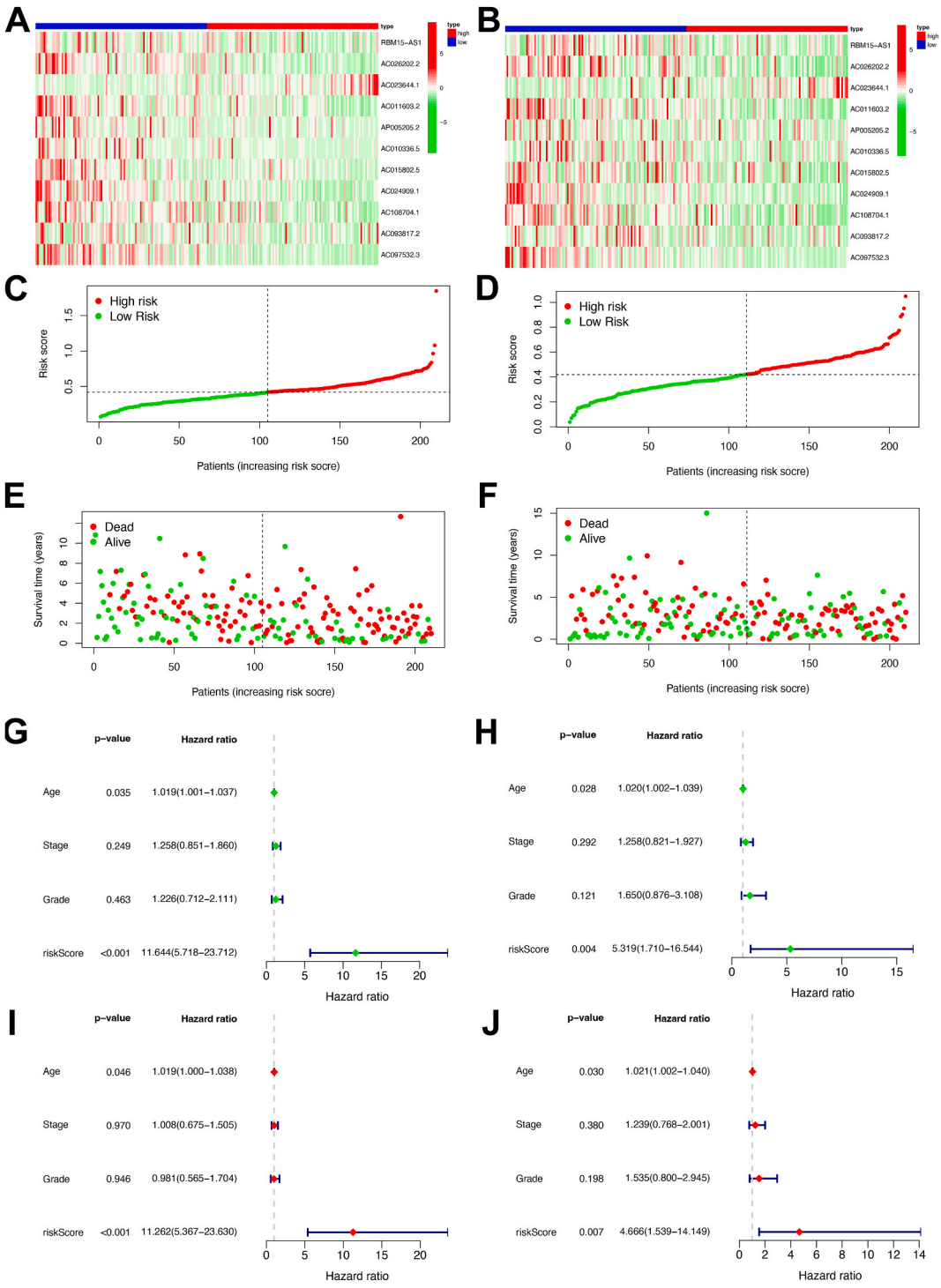

Fig. 11. Evaluation of the performance of riskScore in predicting the survival prognosis of patients with OCa. In the training set (A) and validation set (B), the lncRNA expression paradigms of the high-risk group and the low-risk group were explored respectively. The distribution of riskScore and survival status of OV patients in the training set (C, E) and validation set (D, F). In the training (G, I) and validation sets (H, J), univariate and multivariate cox analysis of Age, Stage, Grade, and riskScore.

cuproptosis inducer, and assessed the viability of si-NC and si-AC023644.1 cells. The results demonstrated that elesclomol could induce cuproptosis in ovarian cancer cells in a concentration-dependent manner. Knocking down AC023644.1 significantly reduced the viability of ovarian cancer cells, but the cells were not sensitive to the cuproptosis inducer (Fig. 15C and D). These results suggest

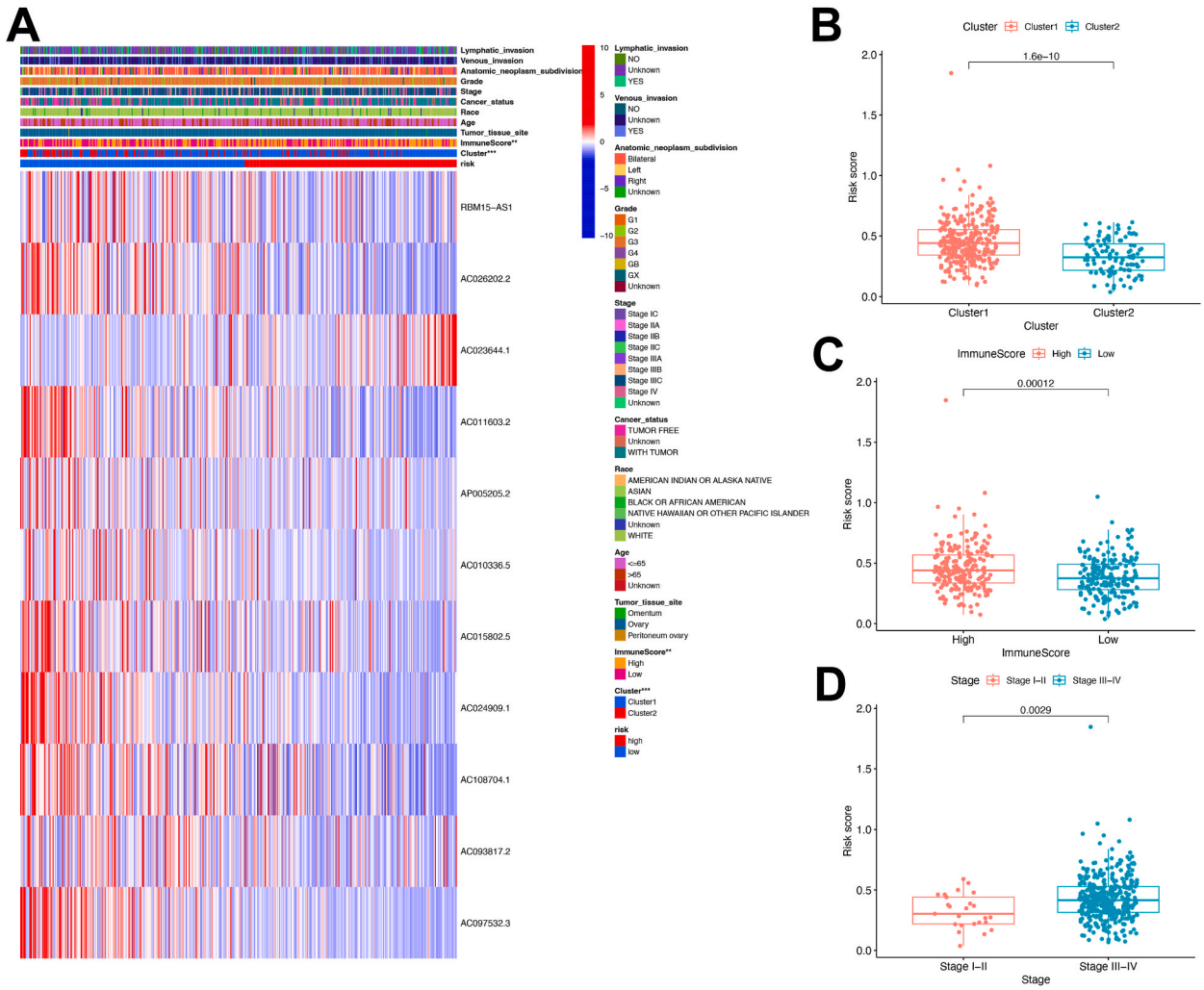

Fig. 12. Comparative analysis of clinical pathological parameters, cuproptosis-related lncRNAs expression level between high-risk and low-risk groups. (A) Heatmap of cuproptosis-related lncRNAs in high-risk and low-risk groups. The difference of riskScore between Cluster1 and Cluster2 groups (B), between high-ImmuneScore and low-ImmuneScore groups (C), and between Stage I-II and Stage III-IV groups (D).

that AC023644.1 may regulate cell viability; however, it remains uncertain whether this regulation involves the cuproptosis mechanism. Further research is needed to determine the impact of AC023644.1 on cuproptosis in ovarian cancer cells.

4. Discussion

In this research, we conducted a comprehensive screening to identify CuLncs, which were utilized to construct a robust prognostic prediction model for OCa. Subsequently, this model was rigorously validated to ensure its reliability and accuracy. Additionally, we meticulously evaluated the differential expression of CuLncs between the high and low riskScore groups, shedding light on the potential molecular mechanisms underlying disease progression. Furthermore, an in-depth analysis of immune infiltration was performed, unraveling the intricate interplay between the immune microenvironment and OCa prognosis. These findings contribute towards our understanding of OCa pathogenesis and may offer valuable insights for developing personalized therapeutic approaches.

The categorization of OCa patients into different clusters based on CuLncs revealed distinct risk values, indicating variations in clinical outcomes. Cluster 1 displayed significantly higher risk values compared to Cluster 2, suggesting a higher likelihood of disease progression and poorer prognosis in the former group. Additionally, the association between higher immune scores and increased risk values implies the involvement of immune response in disease severity, with OCa patients having a more robust immune response potentially experiencing worse clinical outcomes. The tumor-related immune response mechanisms are extremely complex. Our research findings indicate differences in the immune infiltration levels of NK cells resting and Neutrophils between two clusters, which may suggest that these two cell types play important roles in certain molecular mechanisms, regulating the OCa tumor microenvironment, and ultimately leading to differences in the survival of OCa patients. According to literature reports, resting NK cells have

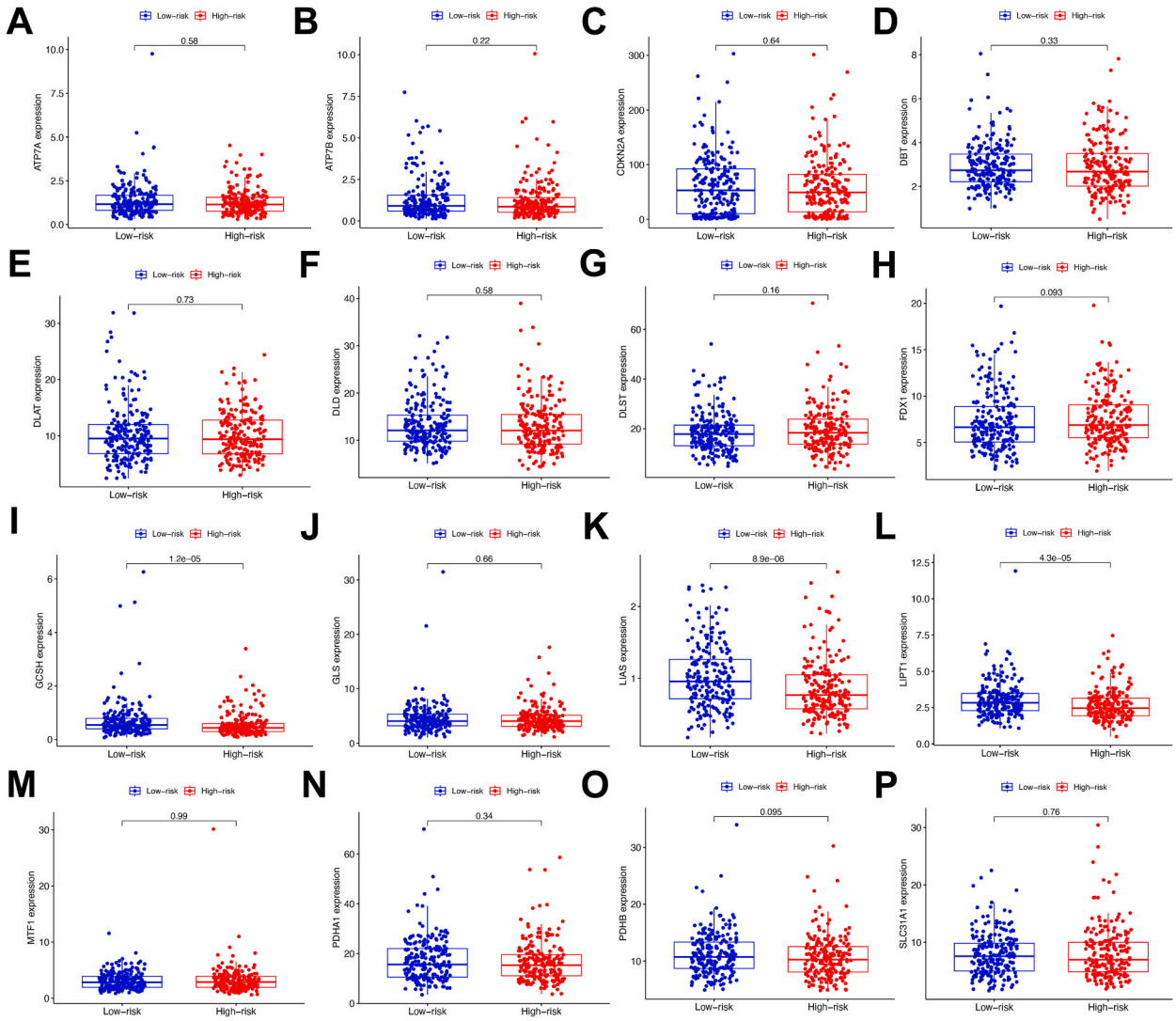

Fig. 13. Differential expression of cuproptosis-related genes between high-risk and low-risk groups.

been found to possess the capability of directly recognizing freshly isolated human tumor cells, specifically identifying ovarian carcinoma as a potential target for adoptive immunotherapy based on NK cells [26]. The findings from Lee et al.'s research suggest a link between the formation of neutrophil extracellular traps (NETs) and the creation of a conducive omental niche for the implantation of OCa cells [27]. This raises the possibility that preventing NET formation could be a viable strategy to inhibit the metastasis of OCa to the omentum. A study presented demonstrates that the activation of neutrophil effector functions in the tumor microenvironment (TME) through complement-dependent pathways induces a distinct T-cell nonresponsiveness [28]. This nonresponsiveness is separate from the established checkpoint pathways typically targeted in immunotherapy. Importantly, the research also identifies specific targets that could be utilized for immunotherapy in OCa. These findings shed light on potential strategies to enhance T-cell responses and improve the effectiveness of immunotherapeutic approaches in OCa.

We utilized LASSO regression analysis to converge the typing model constructed based on CuLncs, thereby avoiding overfitting. Ultimately, we obtained an OCa prognosis risk scoring model based on 11 key CuLncs. The model accurately predicts the survival rates of OCa patients at 1, 3, and 5 years by calculating the riskScore, which is beneficial for the survival assessment of OCa patients. However, the mechanisms and functions of these 11 CuLncs in cuproptosis and the occurrence and progression of OCa have not been reported or understood yet. In the present study, we preliminarily explored the effect of AC023644.1 on the viability of OCa cells and found that knocking down AC023644.1 led to a decrease in OCa cell viability. This indicates that AC023644.1 can regulate the proliferation of OCa cells. Survival analysis results suggest that AC023644.1 is a risk factor for the survival of OCa patients. The potential mechanism might be that high levels of AC023644.1 expression inhibit the death of OCa cells. However, it remains unclear whether part of this effect is achieved through the regulation of the cuproptosis process, which requires further in-depth investigation. Interestingly, in OCa cells with AC023644.1 knocked down, the concentration-dependent cuproptosis induced by elesclomol

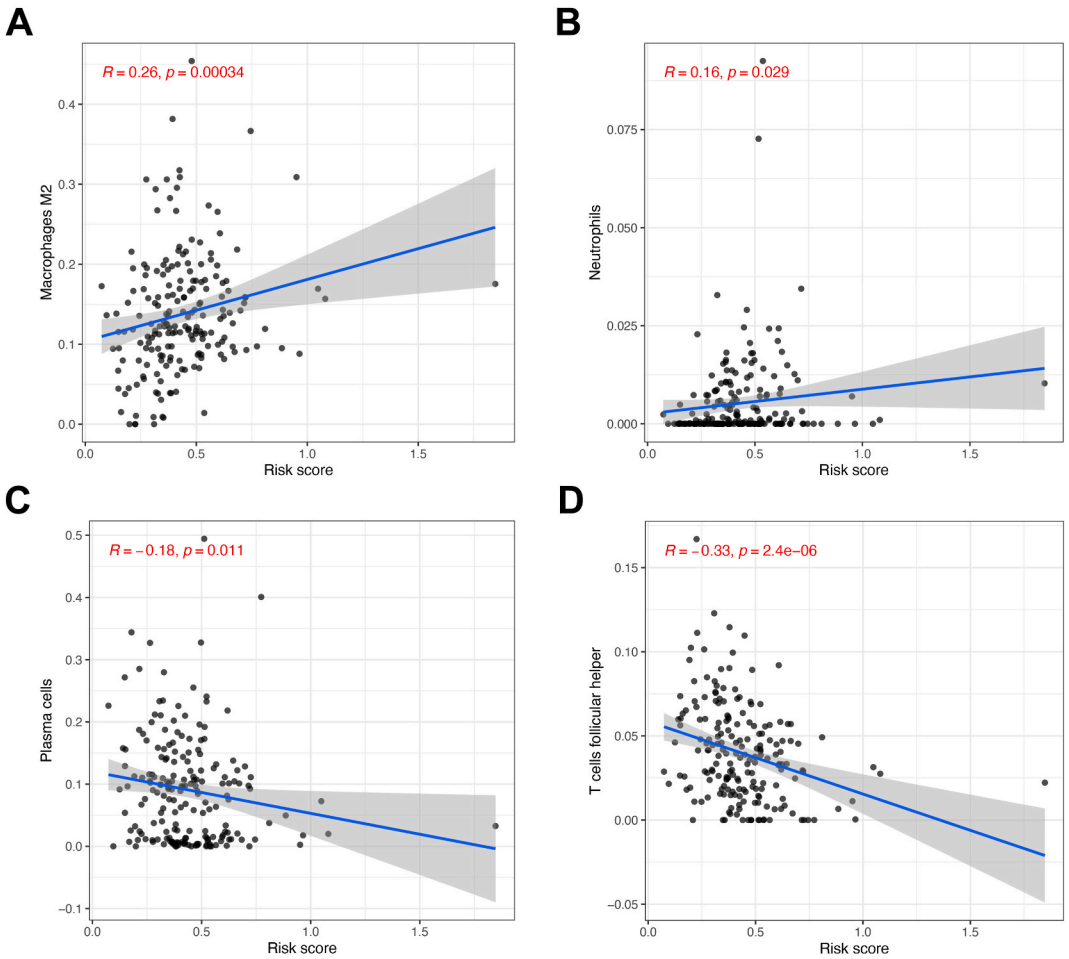

Fig. 14. Correlation analysis of immune cell infiltration degree and riskScore. Scatter plot of correlation analysis between Plasma cells (A), Macrophages M2 (B), T cells follicular helper (C), Neutrophils (D) and riskScore.

disappeared. We speculate that knocking down AC023644.1 may affect the sensitivity of OCa cells to elesclomol. The specific mechanism requires further investigation.

The examination of CRGs expression patterns in the high-risk and low-risk groups revealed significant differences in the expression levels of GCSH, LIAS, and LIPT1. A recent study found that the GCSH is overexpressed in breast cancer cells and tissue, while a shorter transcript variant (Tv*) is amplified in healthy breast cells but decreased in breast cancer samples. The balance between the two variants plays a crucial role in cancer cell viability, with Tv* overexpression leading to decreased metabolic activity and necrosis, while the protein-coding transcript variant 1 (Tv1) overexpression increases cellular vitality and mitochondrial glycine decarboxylation activity [29]. This indicates that GCSH regulation is important in determining cancer cell viability. The study by Cai et al. demonstrated that LIAS plays a crucial role in cancer progression [30]. They conducted comprehensive pan-cancer analyses using bioinformatics platforms such as TIMER2.0, GEPIA2.0, and HPA to investigate the expression levels and prognostic values of LIAS. The findings showed that high LIAS expression is associated with a favorable prognosis in kidney renal clear cell carcinoma, rectum adenocarcinoma, breast cancer, and OCa patients, while high expression is linked to an unfavorable prognosis in lung cancer patients. Additionally, the study revealed that LIAS expression is implicated in hypoxia, angiogenesis, DNA repair, and can serve as a predictor of immunotherapy efficacy in cancer patients. Yan et al. discovered that suppressing the expression of the LIPT1 gene inhibited the proliferation and invasion of hepatoma cells [31]. The findings suggest that LIPT1 could be a promising target for therapeutic intervention in hepatocellular carcinoma. These genes might play crucial roles in OCa development and progression, making them potential prognostic markers and therapeutic targets. Further investigation is necessary to elucidate the specific mechanisms through which these genes contribute to disease pathogenesis and cuproptosis. Additionally, these prognostic markers need to be evaluated in independent cohorts to assess their reliability and potential clinical utility.

The highly immunosuppressive TME and the low mutational burden of OCa present significant challenges to effective treatment [32]. Inhibitory cells within the TME, including myeloid-derived suppressor cells (MDSCs) and tumor-associated macrophages (TAMs), play a crucial role in promoting tumor growth through various suppressive mechanisms. In our study, the correlation analysis between immune cell infiltration and riskScore provided valuable insights into the immune landscape of OCa. Macrophages M2 and

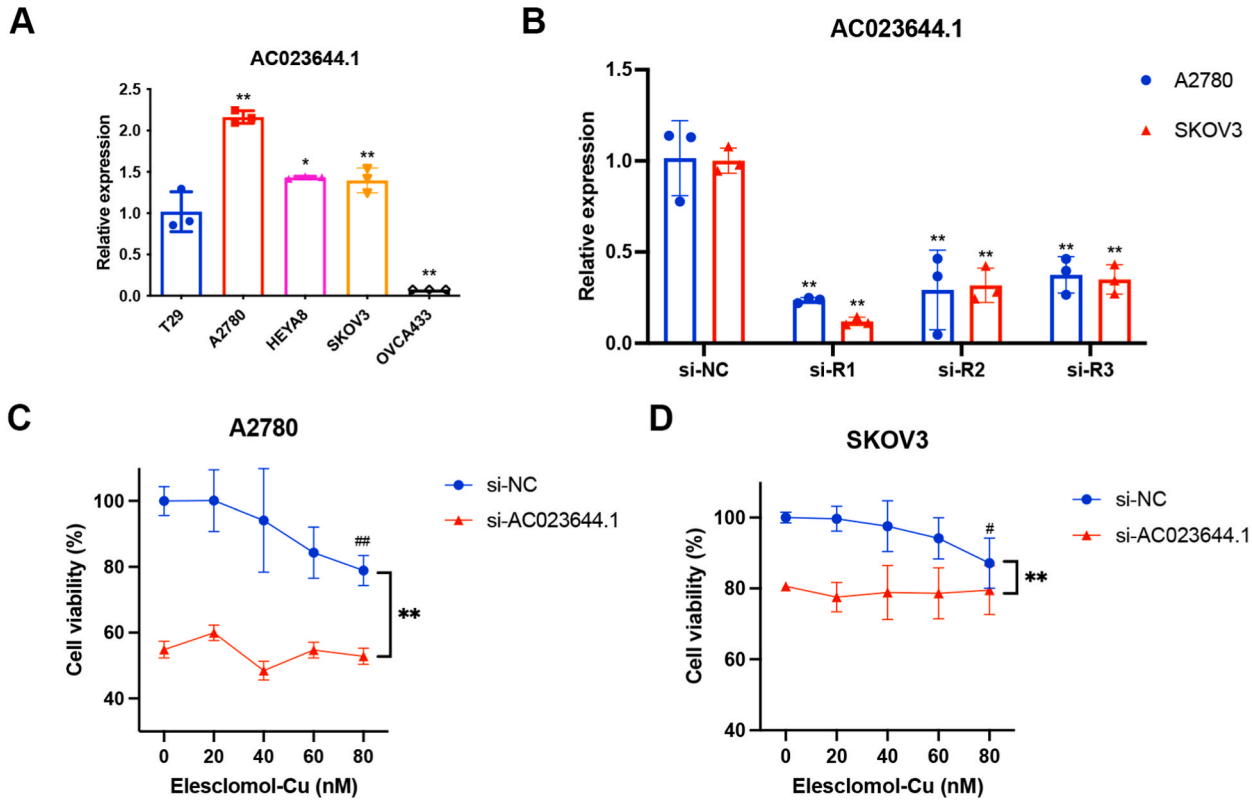

Fig. 15. Knockdown of AC023644.1 inhibits ovarian cancer cell viability and confers insensitivity to cuproptosis inducer. (A) Expression levels of AC023644.1 in normal ovarian epithelial cells (T29) and ovarian cancer cells (A2780, HEYA8, SKOV3, OVCA433). (B) Knockdown efficiency of siRNA detected by RT-qPCR. Elesclomol induces cuproptosis in a concentration-dependent manner in A2780 cells (C) and SKOV3 cells (D), while knockdown of AC023644.1 renders these cells insensitive to cuproptosis inducer.

Neutrophils exhibited a significant positive correlation with riskScore, suggesting their association with tumor progression and immune evasion. Ovarian cancer's resistance to existing immunotherapies is largely influenced by the TME and the presence of immunosuppressive cells, which prevent T cell infiltration and dampen anti-tumor responses [33]. As a result, strategies focused on depleting or reprogramming TAMs to boost T cell activity have become a critical area of research for improving the efficacy of cancer immunotherapy [34]. Conversely, Plasma cells and T cells follicular helper (Tfh) displayed a significant negative correlation with riskScore, indicating a potential protective role against OCa. Previous research indicates that higher levels of Tfh cells in solid organ tumors not derived from lymphocytes frequently correlate with improved prognosis [35–37]. Enhancing or increasing the proportion of Tfh cells in the TME may represent a promising therapeutic approach for treating OCa. These findings highlight the complexity of the tumor microenvironment and the crucial impact of immune cell subsets on disease progression.

Our study has several limitations. For instance, we did not conduct cell experiments to validate the key immune cell subtypes within the TME. Additionally, while we acknowledge that CuLncs signatures have been investigated in prior studies, our research offers distinct contributions in several aspects. Firstly, we screened CuLncs based on 16 cuproptosis-related genes, resulting in a more comprehensive set of candidate genes compared to previous studies, such as the one conducted by Liu et al. [6]. This approach allowed us to identify a broader and potentially more significant array of CuLncs. Furthermore, we examined CuLncs-based cluster types, which provides an additional layer of analysis to our study. This exploration of cluster types could offer deeper insights into the functional roles and interactions of CuLncs in the context of cuproptosis. Further research is warranted to validate our findings in independent cohorts and gain a comprehensive understanding of the functional role of the identified CuLncs and immune cell subsets in OCa. Exploring novel immunotherapeutic approaches, particularly those aimed at modulating the TME or enhancing T cell responses, holds promise for overcoming current treatment limitations. These avenues of research are crucial for addressing gaps in knowledge and ultimately enhancing patient outcomes in OCa. Collectively, our results provide a foundation for future studies aiming to improve diagnosis, prognosis, and personalized treatment approaches for OCa patients.

Funding information

This study received financial backing from the Key Medical Specialty program funded by Shanghai Fifth People's Hospital, Fudan University (grant no. 2020WYZDZK13).

Patient consent for publication

Not applicable.

Ethics statement

Not applicable.

Data availability statement

The code and data for the bioinformatics analysis in this article can be downloaded from the following URL: https://github.com/znxfdd/papercodes. The cell experiments data and materials included in present study are available from the corresponding author upon reasonable request.

CRediT authorship contribution statement

Rujun Chen: Writing – original draft, Visualization, Validation, Investigation, Formal analysis, Conceptualization. **Yating Huang:** Writing – original draft, Validation, Investigation, Data curation. **Ke Sun:** Validation, Investigation, Conceptualization. **Fuyun Dong:** Validation, Investigation, Data curation. **Xiaoqin Wang:** Validation, Investigation. **Junhua Guan:** Formal analysis. **Lina Yang:** Writing – review & editing, Supervision. **He Fei:** Writing – review & editing, Visualization, Supervision, Conceptualization.

Declaration of competing interest

The authors declare that they have no known competing financial interests or personal relationships that could have appeared to influence the work reported in this paper.

Appendix A. Supplementary data

Supplementary data to this article can be found online at https://doi.org/10.1016/j.heliyon.2024.e35004.

References

[1] H. Sung, et al., Global cancer statistics 2020: GLOBOCAN estimates of incidence and mortality worldwide for 36 cancers in 185 countries, CA Cancer J Clin 71 (3) (2021) 209–249.
[2] J. Xie, et al., Cuproptosis: mechanisms and links with cancers, Mol. Cancer 22 (1) (2023) 46.
[3] P.E. Saw, et al., Non-coding RNAs: the new central dogma of cancer biology, Sci. China Life Sci. 64 (1) (2021) 22–50.
[4] J. Shen, et al., Construction of a cuproptosis-associated lncRNA prognostic signature for bladder cancer and experimental validation of cuproptosis-related lncRNA UBE2Q1-AS1, Front. Med. 10 (2023) 1222543.
[5] N. Li, et al., Molecular characterization of cuproptosis-related lncRNAs: defining molecular subtypes and a prognostic signature of ovarian cancer, Biol. Trace Elem. Res.202(4) (2024) 1428–1445.
[6] L. Liu, et al., Developing four cuproptosis-related lncRNAs signature to predict prognosis and immune activity in ovarian cancer, J. Ovarian Res. 16 (1) (2023) 88.
[7] X. Mo, et al., A novel cuproptosis-related prognostic lncRNA signature and lncRNA MIR31HG/miR-193a-3p/TNFRSF21 regulatory axis in lung adenocarcinoma, Front. Oncol. 12 (2022) 927706.
[8] B. Guo, et al., Cuproptosis induced by ROS responsive nanoparticles with elesclomol and copper combined with αpd-L1 for enhanced cancer immunotherapy, Adv. Mater. 35 (22) (2023) e2212267.
[9] W.Q. Liu, et al., Copper homeostasis and cuproptosis in cancer immunity and therapy, Immunol. Rev. 321 (1) (2024) 211–227.
[10] X. Nie, et al., Anisomycin has a potential toxicity of promoting cuproptosis in human ovarian cancer stem cells by attenuating YY1/lipoic acid pathway activation, J. Cancer 13 (14) (2022) 3503–3514.
[11] J. Guo, Y. Sun, G. Liu, The mechanism of copper transporters in ovarian cancer cells and the prospect of cuproptosis, J. Inorg. Biochem. 247 (2023) 112324.
[12] K. Wang, et al., Multi-omics analysis defines a cuproptosis-related prognostic model for ovarian cancer: implication of WASF2 in cuproptosis resistance, Life Sci. 332 (2023) 122081.
[13] J. Yang, et al., ACE2 correlated with immune infiltration serves as a prognostic biomarker in endometrial carcinoma and renal papillary cell carcinoma: implication for COVID-19, Aging (Albany NY) 12 (8) (2020) 6518–6535.
[14] P. Tsvetkov, et al., Copper induces cell death by targeting lipoylated TCA cycle proteins, Science 375 (6586) (2022) 1254–1261.
[15] T.M. Therneau, P.M. Grambsch, Modeling Survival Data: Extending the Cox Model, Springer, New York, 2013.
[16] M.D. Wilkerson, D.N. Hayes, ConsensusClusterPlus: a class discovery tool with confidence assessments and item tracking, Bioinformatics 26 (12) (2010) 1572–1573.
[17] L.J.A. Stalpers, E.L. Kaplan, Edward L. Kaplan, The kaplan-meier survival curve, J. Pers. Interpers. Loss: Journal of the British Society for the History of Mathematics 33 (2) (2018) 109–135.
[18] P. Blanche, J.F. Dartigues, H. Jacqmin-Gadda, Estimating and comparing time-dependent areas under receiver operating characteristic curves for censored event times with competing risks, Stat. Med. 32 (30) (2013) 5381–5397.
[19] R. Kolde, pheatmap: Pretty Heatmaps. R package version 1.0. 12 (2019).
[20] A. Subramanian, et al., Gene set enrichment analysis: a knowledge-based approach for interpreting genome-wide expression profiles, Proc. Natl. Acad. Sci. USA 102 (43) (2005) 15545–15550.
[21] M.E. Ritchie, et al., Limma powers differential expression analyses for RNA-sequencing and microarray studies, Nucleic Acids Res. 43 (7) (2015) e47.
[22] B. Chen, et al., Profiling tumor infiltrating immune cells with CIBERSORT, Methods Mol. Biol. 1711 (2018) 243–259.

[23] N. Winter, VIOPLOT: Stata Module to Produce Violin Plots with Current Graphics, 2008.
[24] H. Wickham, ggplot2: Elegant Graphics for Data Analysis, Springer International Publishing, 2016.
[25] J. Liu, et al., A genetically defined model for human ovarian cancer, Cancer Res. 64 (5) (2004) 1655–1663.
[26] M. Carlsten, et al., DNAX accessory molecule-1 mediated recognition of freshly isolated ovarian carcinoma by resting natural killer cells, Cancer Res. 67 (3) (2007) 1317–1325.
[27] W. Lee, et al., Neutrophils facilitate ovarian cancer premetastatic niche formation in the omentum, J. Exp. Med. 216 (1) (2019) 176–194.
[28] T.R. Emmons, et al., Mechanisms driving neutrophil-induced T-cell immunoparalysis in ovarian cancer, Cancer Immunol. Res. 9 (7) (2021) 790–810.
[29] A. Adamus, et al., GCSH antisense regulation determines breast cancer cells' viability, Sci. Rep. 8 (1) (2018) 15399.
[30] Y. Cai, et al., Comprehensive analysis of the potential cuproptosis-related biomarker LIAS that regulates prognosis and immunotherapy of pan-cancers, Front. Oncol. 12 (2022) 952129.
[31] C. Yan, et al., System analysis based on the cuproptosis-related genes identifies LIPT1 as a novel therapy target for liver hepatocellular carcinoma, J. Transl. Med. 20 (1) (2022) 452.
[32] J. Liu, J. Zhu, Progresses of T-cell-engaging bispecific antibodies in treatment of solid tumors, Int Immunopharmacol 138 (2024) 112609.
[33] J. Chen, et al., Recent advances in understanding the immune microenvironment in ovarian cancer, Front. Immunol. 15 (2024) 1412328.
[34] Z. Li, et al., Tumor-associated macrophages in anti-PD-1/PD-L1 immunotherapy for hepatocellular carcinoma: recent research progress, Front. Pharmacol. 15 (2024) 1382256.
[35] X. Lin, et al., Follicular helper T cells remodel the immune microenvironment of pancreatic cancer via secreting CXCL13 and IL-21, Cancers 13 (15) (2021).
[36] D. Baumjohann, P. Brossart, T follicular helper cells: linking cancer immunotherapy and immune-related adverse events, J Immunother Cancer 9 (6) (2021).
[37] C. Gu-Trantien, et al., CD4^{+} follicular helper T cell infiltration predicts breast cancer survival, J. Clin. Invest. 123 (7) (2013) 2873–2892.